INL/RPT-22-68273
Revision 0

Comparison of Irradiated and Unirradiated Graphite Oxidation Performance

July 2022

Split Samples of NBG-25 Graphite after Exposure of up to 6.8 dpa Irradiation

Rebecca E. Smith
Staff Engineer, Materials Properties & Performance

Idaho National Laboratory

INL is a U.S. Department of Energy National Laboratory operated by Battelle Energy Alliance, LLC

INL/RPT-22-68273
Revision 0

Comparison of Irradiated and Unirradiated Graphite Oxidation Performance

Split Samples of NBG-25 Graphite after Exposure of up to 6.8 dpa Irradiation

Rebecca E. Smith
Staff Engineer, Materials Properties & Performance

July 2022

Idaho National Laboratory
Advanced Reactor Technologies
Idaho Falls, Idaho 83415

http://www.art.inl.gov

Prepared for the
U.S. Department of Energy
Office of Nuclear Energy
Under DOE Idaho Operations Office
Contract DE-AC07-05ID14517

Page intentionally left blank

INL ART Program

Comparison of Irradiated and Unirradiated Graphite Oxidation Performance

INL/RPT-22-68273
Revision 0

July 2022

Technical Reviewer: (Confirmation of mathematical accuracy, and correctness of data and appropriateness of assumptions.)

	7/28/2022
Joseph L. Bass Computational Materials Scientist	Date

Approved by:

	7/2/2022
William E. Windes ART Graphite R&D Technical Lead	Date
M. Davenport	7/28/2022
Michael E. Davenport ART Project Manager	Date
Michelle Sharp	7/28/2022
Michelle T. Sharp INL Quality Assurance	Date

Page intentionally left blank

ABSTRACT

This work examines the oxidation behavior of NBG-25 graphite using irradiated specimens and (unirradiated) companion specimens from the Advanced Graphite Creep (AGC) Experiment. Irradiated and companion specimens were quartered into four small split samples to enable four oxidation test runs for each (0.5-inch diameter by 0.25-inch tall) piggyback button obtained from the AGC Experiment inventory. These split samples were oxidized in air in a thermogravimetric analyzer (TGA) and benchmarked against observations with separately sourced same-grade specimens of three geometries oxidized either in the TGA or in a vertical furnace built and operated to satisfy the specifications of ASTM D7542. The study considers both irradiation damage and relief of damage by thermal annealing. A range of isothermal oxidation temperatures was tested for specimens exposed to a similar irradiation environment, nominally 6.5 dpa at 650°C. To assess the dose dependency of observed oxidation behavior, specimens with a range of irradiation exposures (up to 6.8 dpa) were tested at the single oxidation temperature of 650°C. In the conventional analysis (rate determined over the 5–10% mass loss range) any annealing effects appear to be negligible, while irradiation to ~6.5 dpa may double or triple the subsequent oxidation rate. However, examination of rate with extent of reaction (over incremental ranges from initial onset up to 5% mass loss) illustrates that (at least for ~6.5 dpa) irradiation initially inhibits oxidation. Slower rates of oxidation compared with companion split samples were clearly indicated across all oxidation temperatures tested up to ~0.5% mass loss. Over the range of 0.5–1% mass loss, regardless of normalization strategy, there is no statistically meaningful difference in oxidation rate. However, beyond 0.5% mass loss oxidation of the irradiated sample becomes progressively faster than the companion sample (up to the 10% mass loss level observed).

Page intentionally left blank

ACKNOWLEDGEMENTS

The author would like to recognize W. D. Swank (retired), D. C. Haggard (retired), D. L. Cottle, and A. C. Matthews of Idaho National Laboratory (INL) for their many contributions to the success of this experimental testing effort. Special thanks are also offered to Josh Kane of INL, to Cristian Contescu (retired) and Ryan Paul of Oak Ridge National Laboratory and to consultant Martin Metcalfe of the United Kingdom for helpful recommendations in the analysis and interpretation of these results.

Page intentionally left blank

CONTENTS

FIGURES

TABLES

Page intentionally left blank

ACRONYMS

AGC	Advanced Graphite Creep
TGA	thermogravimetric analyzer

Page intentionally left blank

Comparison of Irradiated and Unirradiated Graphite Oxidation Performance

1. INTRODUCTION

Oxidation of graphite (in air, steam, or carbon dioxide) is a heterogeneous chemical reaction that leads to mass loss from the graphite. In the reacting material, mass loss rate and distribution are both of interest because they directly influence the risks associated with degradation of properties significant to the functionality of the material (Contescu 2010; Kane 2017). In the extreme, either acute or chronic oxidation can be problematic, with damage to mechanical strength posing a significant concern for nuclear safety (Windes 2014). The focus of this work is on acute oxidation in air for the purpose of building an understanding of how neutron irradiation of graphite influences the rate of its subsequent oxidation. While not within the scope of this experiment, the distribution of mass loss during oxidation is important context for data analysis (evolution of a density gradient relative to the size and geometry of the article) (Kim 2006; Wichner 2009).

Experimental control of graphite oxidation requires consistent control of both the test specimen and environmental parameters. (Kim 2006; Chi 2015). Temperature, gas flow rate, concentration of oxidant, specimen geometry, extent of reaction, and grade of graphite are all known to be significant to the rate of reaction (Contescu 2008). The history of an article of graphite can have profound effects on the microstructure, with grade differences among as-manufactured graphite and the extent of oxidation being two prime examples where both microstructure influences oxidation rate and vice versa (Contescu 2011). Although there are few studies regarding oxidation after irradiation, (Kosiba 1959; Dahl 1961; Zherdev 1992), irradiation of graphite is known to cause significant microstructural changes deemed likely to affect oxidation, including alteration of the pore structure (porosity being the inverse of density) and the generation of defects (by displacement of carbon) (Kelly 2000; Chinnathambi 2015). Studies suggest that annealing of graphite may heal such defects (Dahl 1961; Schweitzer 1965). Given the elevated temperatures required for the testing of oxidation, annealing was explicitly controlled in an early test set. Specimens from a single graphite grade, NBG-25, from the Advanced Graphite Creep (AGC) Experiment (irradiated and not) and from separately sourced (not irradiated) NBG-25 were employed. Annealing and irradiation (up to 6.5 dpa) dose histories are considered separately and together for their effects on the air oxidation rate.

For control of the oxidizing environment, a thermogravimetric analyzer (TGA) was operated as an analog to the vertical furnace system described in the *Standard Test Method for Air Oxidation of Carbon and Graphite in the Kinetic Regime* (ASTM D7542): an isothermal test temperature was attained in nitrogen before switching to dry air. The graphite sample was suspended on an open-weave basket to allow unimpeded exposure of the specimen to the oxidizing gas flow. Test temperatures were selected to maintain a linear Arrhenius relationship under kinetic reaction control. The (maximum available) gas flow rate of 200 mL/minute was used, as previously determined to provide comparable results to vertical furnace operation for button specimens, cylindrical specimens 12.7 mm in diameter by 6.4 mm (Smith 2019).

Because irradiated graphite test materials are in limited supply and because adequate information to evaluate graphite oxidation requires testing at multiple temperatures, button specimens (with an axial hole, 2-mm diameter) were cut to produce four split specimens (Figure 1).

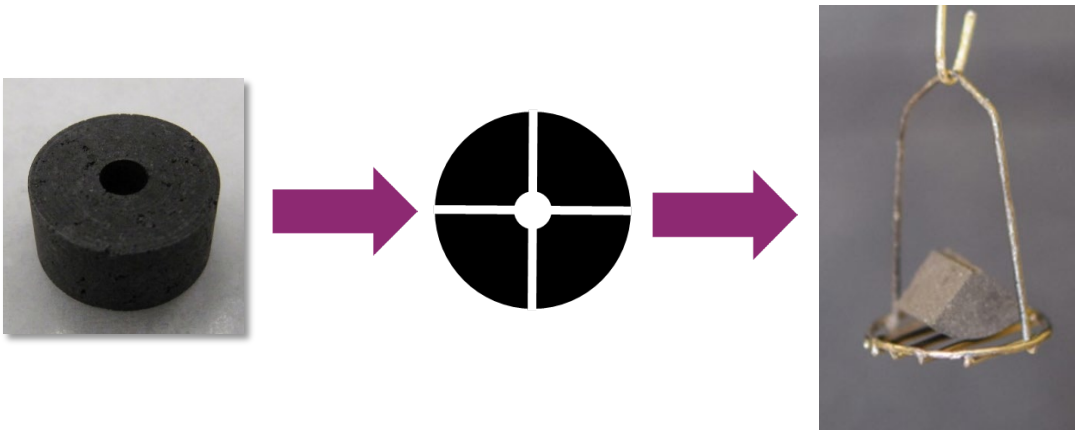

Figure 1. Button samples, sized as AGC piggyback specimens (left image) are cut into four split samples for oxidation testing. A single split sample as suspended for testing in the TGA (right image).

NBG-25 graphite samples were selected to provide enough test material of a single grade with approximately the same irradiation dose and irradiation temperature history to enable comparison of the resultant Arrhenius relationship over a meaningful range of oxidation temperatures. Oxidation test temperatures of 600°C, 620°C, 650°C, 680°C, and up to 700°C were used to assure a linear Arrhenius relation governed by chemical kinetics comparable to testing of much larger specimens under the *Standard Test Method for Air Oxidation of Carbon and Graphite in the Kinetic Regime* (ASTM D7542). AGC graphite companion buttons were used to provide same-source NBG-25 for control specimens that were not irradiated. Separately sourced NBG-25 graphite was also tested to provide additional confidence in the TGA test methodology. Further testing at the single 650°C oxidation temperature examined the performance of split samples reflecting a spectrum of irradiation histories to illustrate dose dependency. See Table 1 for a summary of test materials. See Table 2 for a summary of the corresponding whole button dimensional data.

Table 1. NBG-25 Whole Button Histories and Test Objectives.

Control History and Test Purpose	DPA	Irradiation Temperature (°C)	Intended Oxidation Temperature (°C)
~6.5 dpa Dose with and without anneal	6.78	678.5	600
	6.5	650.3	620
	6.7	665.9	650
	6.2	628.9	650
	6.84	680.0	650
	6.36	658.0	680
	6.82	675.9	700
No irradiation, with and without anneal, AGC Companions	0	Not Applicable	600
	0		620
	0		620
	0		650
	0		650
	0		680
	0		680
No irradiation, with and without anneal, Separately Sourced NBG-25	0	Not Applicable	620
	0		650
	0		650
Dose Dependency, without anneal	5.43	614.5	650
	4.48	530.1	650
	3.59	485.7	650
	2.52	435.4	650
Follow-on Split Process Control (no irradiation, without anneal) Separately Sourced NBG-25	0	Not Applicable	600
	0		600
	0		680
	0		680

Table 2. NBG-25 Whole Button Dimensional Changes with Irradiation.

Control History and Test Purpose	Dose (dpa)	Irradiation Temperature (°C)	Measurements before Irradiation				Measurements before Splitting			
			Mass (g)	Diameter (mm)	Height (mm)	Axial Hole Diameter (mm)	Mass (g)	Diameter (mm)	Height (mm)	Axial Hole Diameter (mm)
~6.5 dpa Dose with and without anneal	6.78	678.5	1.4508	12.73	6.34	2.09	1.4496	12.56	6.30	1.97
	6.5	650.3	1.4479	12.74	6.31	2.10	1.4467	12.57	6.25	1.97
	6.7	665.9	1.4485	12.73	6.33	2.08	1.4472	12.57	6.29	1.97
	6.2	628.9	1.4436	12.73	6.30	2.10	1.4424	12.57	6.25	1.97
	6.84	680.0	1.4487	12.73	6.33	2.08	1.4401	12.56	6.29	1.97
	6.36	658.0	1.4516	12.73	6.33	2.09	1.4505	12.59	6.28	1.96
	6.82	675.9	1.4503	12.73	6.34	2.08	1.4489	12.56	6.29	1.97
No irradiation, with and without anneal, AGC Companions	0	Not Applicable					1.4579	12.69	6.37	0.00
	0						1.4455	12.73	6.31	2.08
	0						1.4434	12.72	6.33	2.08
	0						1.4435	12.73	6.32	2.08
	0						1.4440	12.72	6.33	2.08
	0						1.3988	12.73	6.33	3.21
	0						1.4000	12.74	6.33	3.22
No irradiation, with and without anneal, Separately Sourced NBG-25	0						1.4400	12.71	6.37	1.99
	0						1.4382	12.71	6.36	1.99
	0						1.4401	12.72	6.35	1.99
Dose Dependency, without anneal	5.43	614.5	1.4524	12.73	6.33	2.08	1.4512	12.61	6.29	1.97
	4.48	530.1	1.4459	12.73	6.30	2.09	1.4448	12.62	6.26	1.96
	3.59	485.7	1.4456	12.74	6.32	2.08	1.4443	12.64	6.28	1.98
	2.52	435.4	1.4437	12.73	6.32	2.10	1.4424	12.67	6.29	1.98
Follow-on Split Process Control (no irradiation, no anneal) Separately Sourced NBG-25	0	Not Applicable					1.4345	12.71	6.37	1.99
	0						1.4346	12.72	6.36	2.02
	0						1.4361	12.71	6.37	1.99
	0						1.4371	12.71	6.37	1.99

Experimental subsets build on successively acquired data to support the following four test objectives. The first subset examines the Arrhenius relationship for materials irradiated to approximately 6.5 dpa and illustrates the influence of annealing and the relative magnitudes of the annealing and irradiation effects on oxidation. The second subset examines the dose relationship with oxidation at a single intermediate temperature (650°C). The third subset validates the testing results by confirming the comparison of split sample test methodology against both the split specimens produced from the AGC companion buttons and existing data for NBG-25 big cylinders (nominally 50.8-mm tall by 25.4-mm diameter) using split samples generated by machining left over NBG-25 big cylinders into buttons and then splitting and testing them in the TGA. Collectively this work illustrates the relative magnitudes of annealing and irradiation on oxidation of NBG-25.

2. ANNEALING EFFECT ON OXIDATION

To determine the annealing effect on oxidation, two of the four split samples generated from the same button in the first test set were annealed for 24 hours at 800°C while the remaining two were not. Both unirradiated and irradiated split samples were handled the same way. The resulting oxidation rate data, generated from the (mass normalized) rates observed between 5% and 10% mass loss, are illustrated in Figure 2. The sum of weights of split samples from the same parent show that typically between 6–11% of the parent material is lost as saw kerf in the splitting process, but the benefit of more test repetitions and oxidation testing across a wider temperature range seems to be a good tradeoff.

Three observations stand out. First, the fit to the trendlines for the split sample Arrhenius data (shown in Figure 2 as R^2, reflecting the Pearson correlation coefficient) are relatively poor for the sets shown compared to similar data for (not irradiated) larger specimens. One unirradiated AGC companion split sample oxidized at a much faster rate than expected for the 620°C test temperature. Similar data sets for a single grade of graphite with controlled test specimen and environmental parameters (for kinetic-dominant oxidation), whether for whole buttons or big cylinders, oxidized in the TGA or in the vertical furnace, typically show values of $0.98 < R^2 < 1.00$ (Smith 2020). Second, any evidence of an effect from annealing is quite small: annealed and not annealed trendlines are very close, particularly considering the observed scatter. Interestingly, annealing seemed to influence the unirradiated split samples to approximately the same degree as the irradiated ones, possibly indicating easing of residual stresses from sizing by the anneal treatment. Third, while the two pairs of trendlines suggest that annealing decreased the oxidation rates slightly at most, irradiation to ~6.5 dpa caused a decisive increase in oxidation rates across the entire range of temperatures tested.

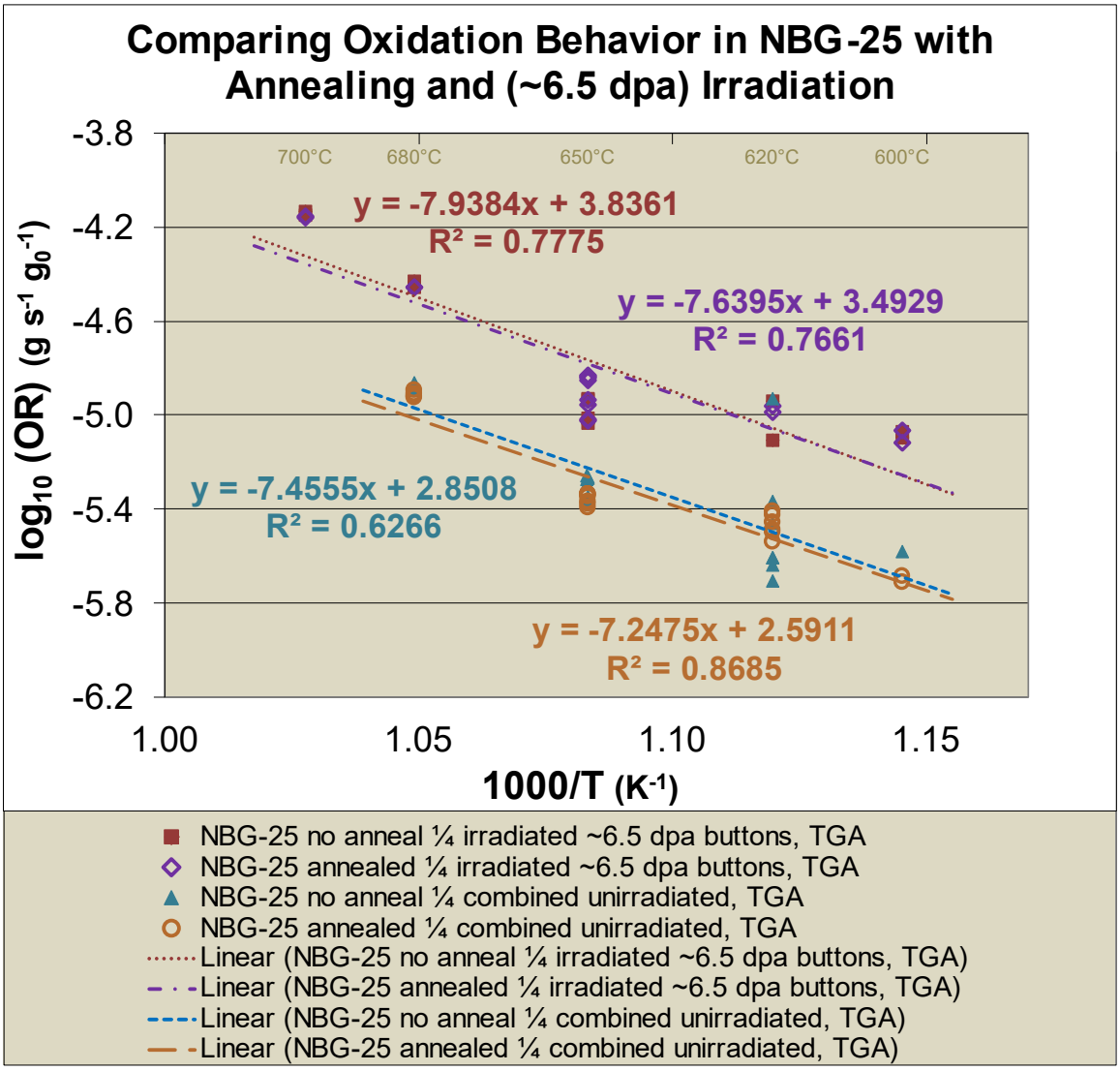

Figure 2. Oxidation performance (at 5–10% mass loss, mass normalized) of unirradiated and irradiated (~6.5 dpa) NBG-25 graphite split samples.

Because one of the AGC companion split samples appears to be an outlier with an inexplicably high oxidation rate (superimposed with the highest rate irradiated split sample tested at 620°C), the AGC companion and separately sourced unirradiated split samples were combined in Figure 2 above, diluting the impact of the one extreme test run for comparison of the trendlines. Individually, these smaller data subsets show too much scatter among too few test temperatures to provide meaningful trends, but consolidating the annealed and not annealed data, the companion and big cylinder sources of unirradiated NBG-25 split samples are illustrated separately in Figure 3. For the following discussion of irradiation effects and dose dependency, annealing and within-grade source distinctions will be neglected.

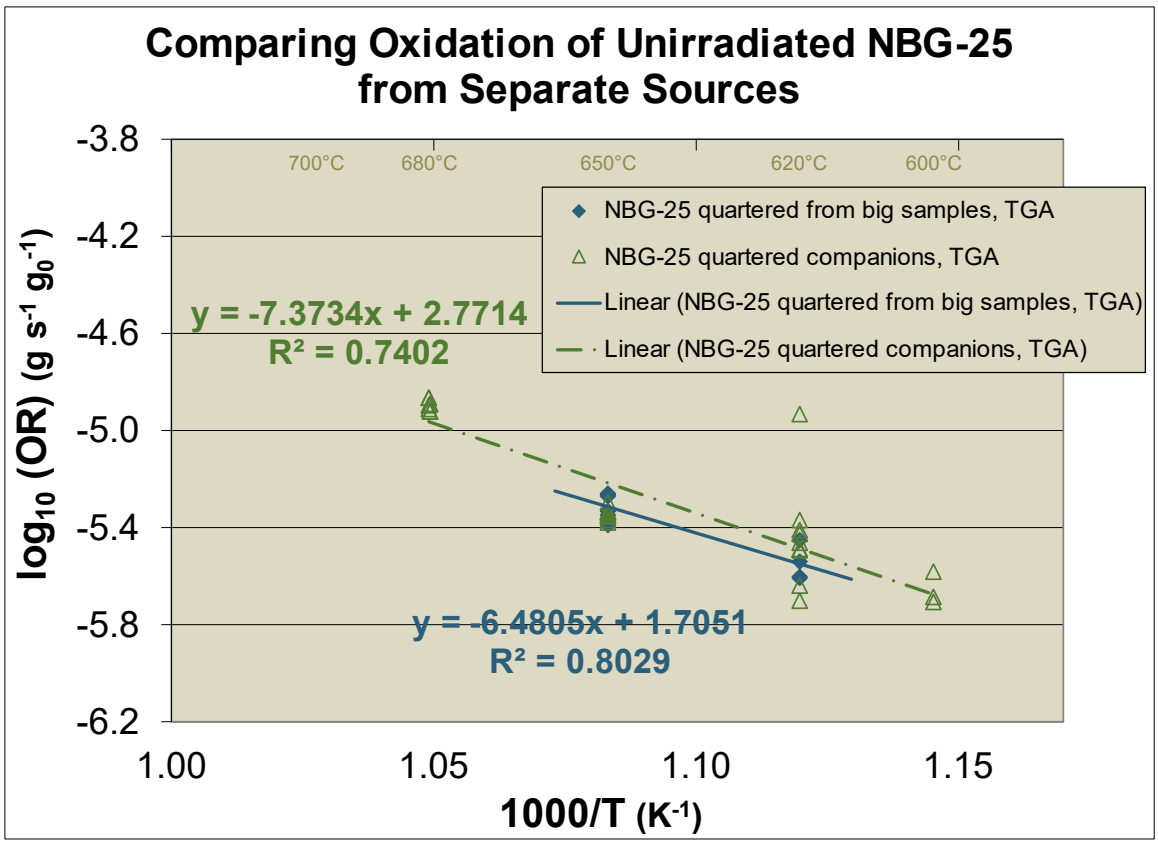

Figure 3. Oxidation data (at 5–10% mass loss, mass normalized) sorted by (same grade, NBG-25) graphite source.

3. IRRADIATION EFFECT ON OXIDATION

3.1 Assessing the Magnitude of the Effect of Irradiation on Oxidation

While the increase in oxidation rate associated with nominal 6.5 dpa neutron irradiation is clearly significant, understanding the magnitude of the observed shift in the Arrhenius plot (Figure 4) in practical terms is more complicated. Even for the irradiated split samples with the most elevated rates of oxidation, the reaction was not self-sustaining. In this sense, they did not burn. Once the run ended and the TGA was no longer maintaining the chamber environment at temperature, the reaction stopped. The logarithmic presentation of oxidation rate can be visually deceptive: mass loss at the lowest of the oxidation temperatures tested more than tripled in rate with 6.36 dpa dose (average duration to 10% mass loss in air at 600°C was 18.6 hours for the companion split samples compared to 1.6 hours for the irradiated) while mass loss for the 680°C test temperature nearly doubled in rate with 6.78 dpa dose (average duration to 10% mass loss in air at 680°C was 2.9 hours for the companion split samples compared to 1.6 hours for the irradiated). Given the scatter in data among all the subsets of split samples, the relative increase in durations to 10% mass loss are indicative of the magnitude of the effect of irradiation on oxidation rate, but ambiguous regarding possible dose dependency.

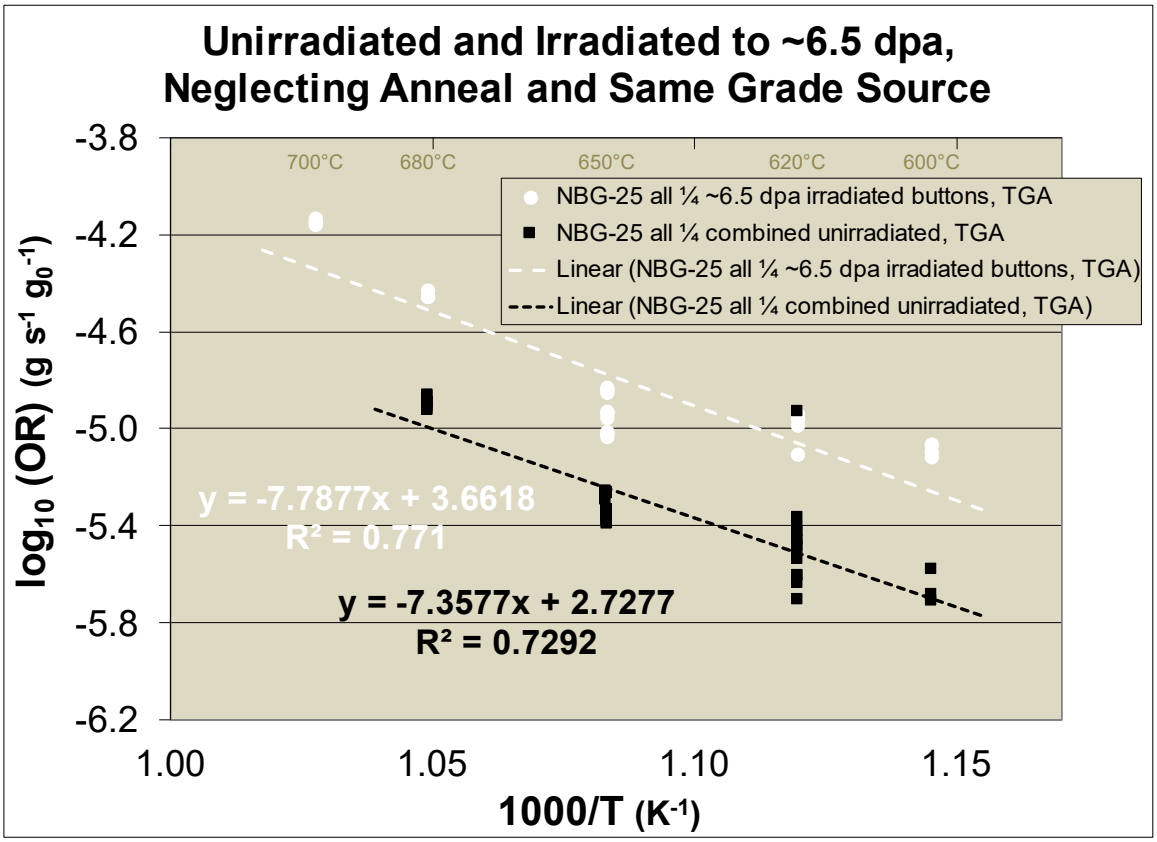

Figure 4. Comparison of oxidation rates of irradiated split samples with a nominal dose of ~6.5 dpa to split samples without any irradiation exposure (at 5–10% mass loss, mass normalized) neglecting both annealing and within-grade source distinctions.

3.2 Dose Dependency of Irradiation Effect

To consider dose dependency, NBG-25 piggyback buttons from the AGC experiment were selected with a range of irradiation histories. These buttons were quartered to provide four split samples for each dose history. Building on the midrange data for ~6.5 dpa and for 0 dpa from the first subset, this second subset of split samples were oxidized in the TGA at 650°C, Figure 5.

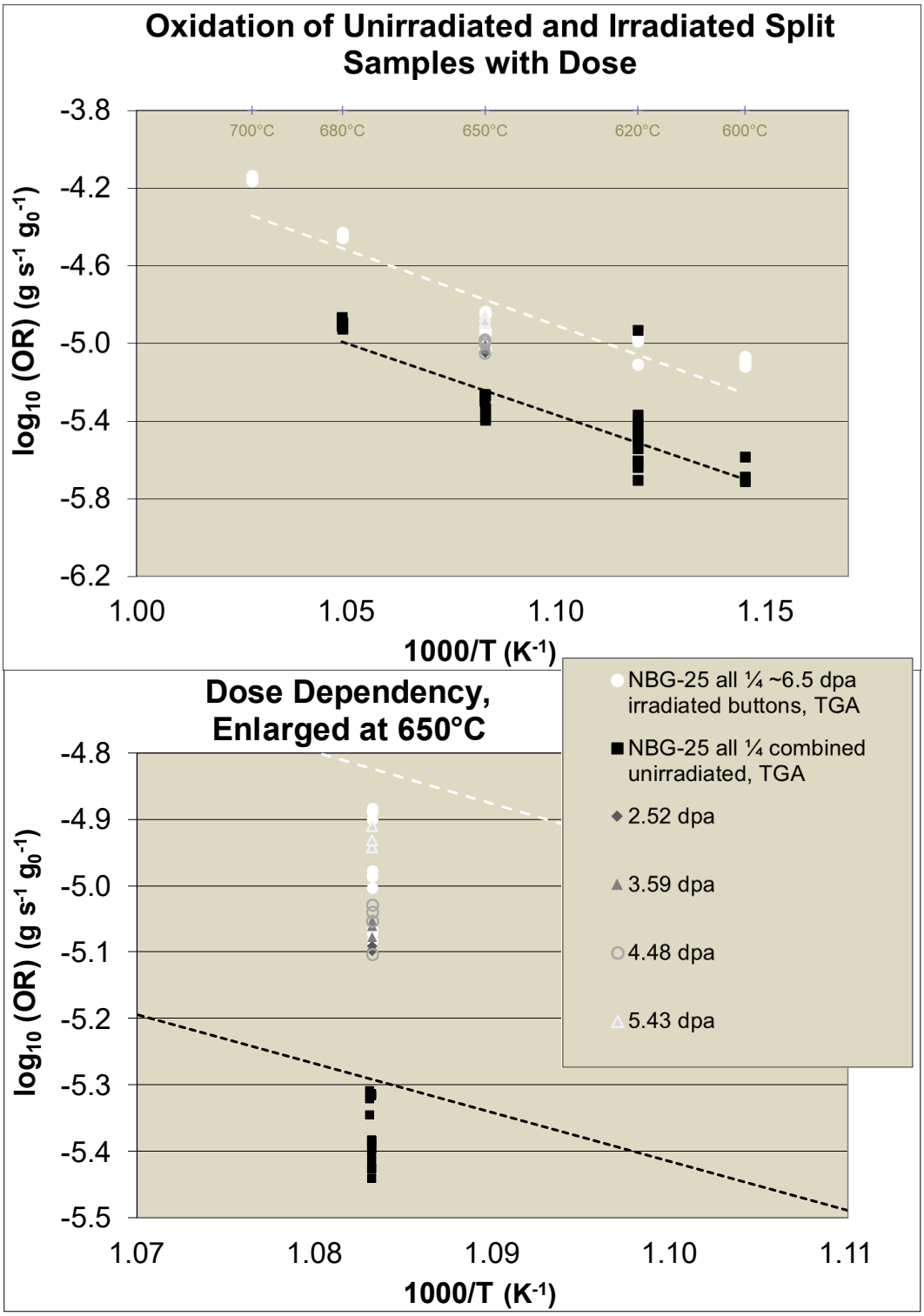

Figure 5. Dose dependency (at 5–10% mass loss, mass normalized) for the exposure range of 0–6.8 dpa, for all temperatures tested (top) and enlarged at 650°C (bottom).

While the collective representation of oxidation with irradiation is hardly more distributed in rate than the scatter in split samples without, (Figure 5, top), the general trend of increasing rate with increasing dose becomes apparent when the graph is enlarged to focus on the results from testing at 650°C (Figure 5, bottom). In the effort to quantify this trend, the oxidation rates (at 5–10% mass loss, mass normalized, in units of g $g_0^{-1}s^{-1}$) are plotted (semi-log scale) with dose, Figure 6. In Figure 6 (left), the results are plotted for each individual sample tested and the relationship seems rather weak. However, when the average oxidation rate is taken for each dose first, and those averaged data are plotted in the same manner, as shown in Figure 6 (right), most of the average oxidation rates appear to be quite close to the resultant trend line. This trend suggests an increase in oxidation rate of approximately 10% for each 1 dpa of irradiation.

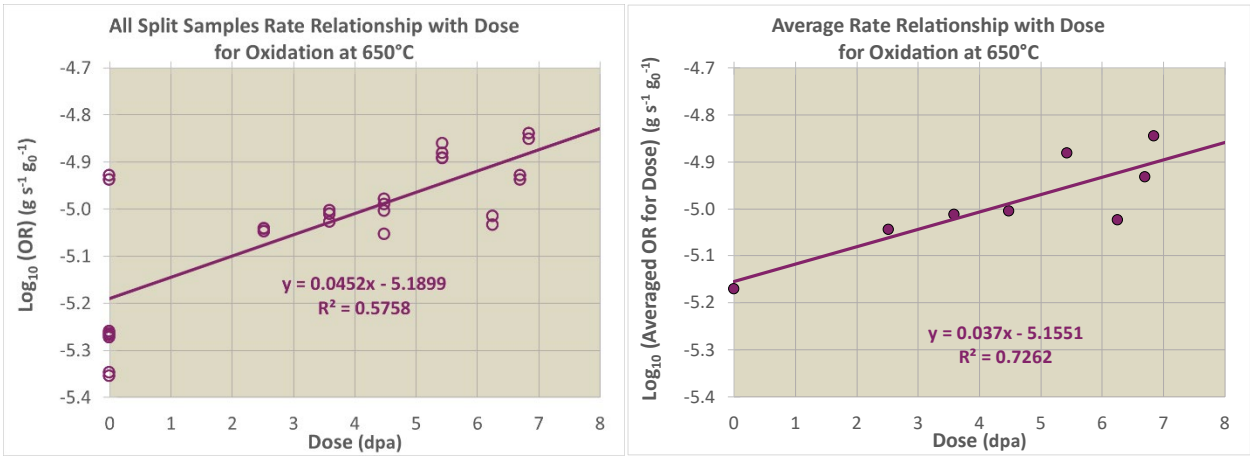

Figure 6. Individual split sample (left) and average-at-dose (right) dose dependency of NBG-25 oxidation rates at 650°C (at 5–10% mass loss, mass normalized).

4. ANALYSIS

Attempting to extrapolate this irradiation effect to larger articles of graphite is convoluted by differences in the test system and its operation, as well as choice of normalization, each of which may produce their own signature influence on the Arrhenius plot (Smith 2019). Over a narrow range of test temperatures, the mass normalized rate behavior of big cylinders and split samples are relatively similar (Figure 7, left), particularly considering the scatter in observed data. However, the effective activation energies (incumbent to the slope of each trend line shown) differ in a manner not obviously accounted for. Figure 7, right, shows similar effective activation energies (~200 kJ/mol) for each subset regardless of sample geometry or test system with comparatively modest variation in the overall mass normalized oxidation behavior between the TGA and vertical furnace systems.

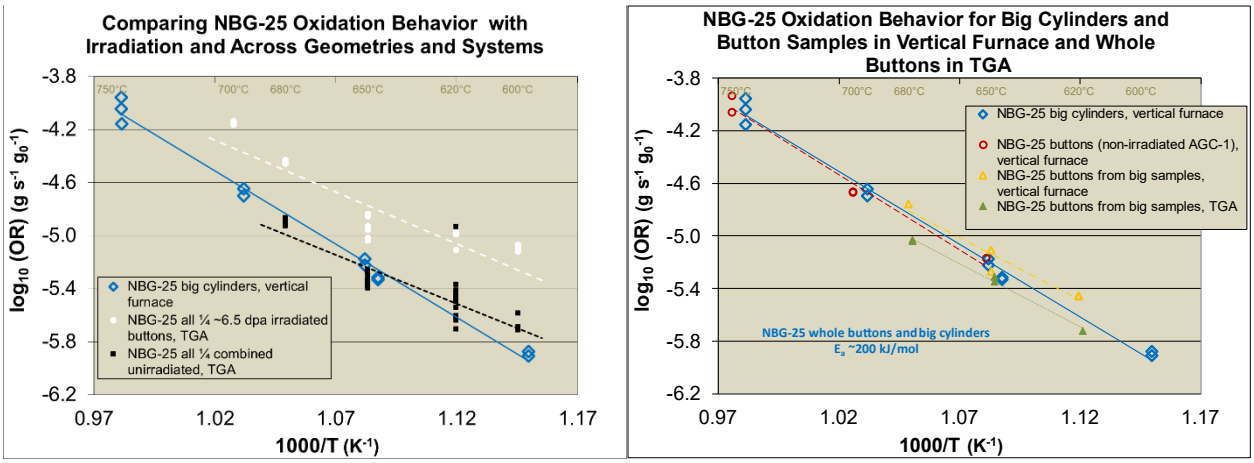

Figure 7. Comparison (at 5–10% mass loss, mass normalized) of NBG-25 split sample oxidation performance in the TGA (with and without irradiation, left) with the performance of NBG-25 subsets previously tested in the vertical furnace and in the TGA (right). Blue diamonds in both left and right graphs represent the same big cylinders oxidized in the vertical furnace.

4.1 Potential for Contaminants

Where both the unirradiated and the irradiated split samples exhibit a parallel reduction in effective activation energy by comparison to all the other oxidation data for larger samples regardless of test system, a concern was identified regarding potential for sample contamination during the splitting process. Experience with oxidation of big cylinder PCEA graphite samples sourced from slabs with and without post-graphitization purification indicated a comparable reduction in effective activation energy associated with the presence of catalytic impurities, Figure 8.

Because contamination with catalytic impurities seemed credible as an explanation for the additional scatter observed in the split sample data as well as the apparent change in effective activation energy, a small follow-on study was performed to assess the splitting process. While a non-metal saw blade proved impractical for this splitting application, a clean metal blade was employed to verify split sample oxidation rates with and without an additional procedural step whereby the split samples were lightly buffed after the cut to remove superficial residue. Four unirradiated NBG-25 buttons (prepared from remaining unused big cylinders) were split with buffed and unbuffed quarters (daughters of the respective parent buttons) tested at 600°C and at 680°C. The results are graphed on top of the earlier NBG-25 split sample data in Figure 9. Oxidation rates for all 16 split specimens in this follow-on effort fell well within the range of results from the earlier unirradiated split samples. Buffing did appear to reduce the scatter in the data slightly, with the buffed samples exhibiting nearly the same average oxidation rate with a fraction of the standard deviation of the unbuffed control at the same oxidation temperature, Table 3. The practice has been adopted for use with future split specimen sample preparation. However, the unbuffed control set shows variance more consistent with larger specimen data sets rather than the R^2 = ~0.7 observed for the earlier split samples.

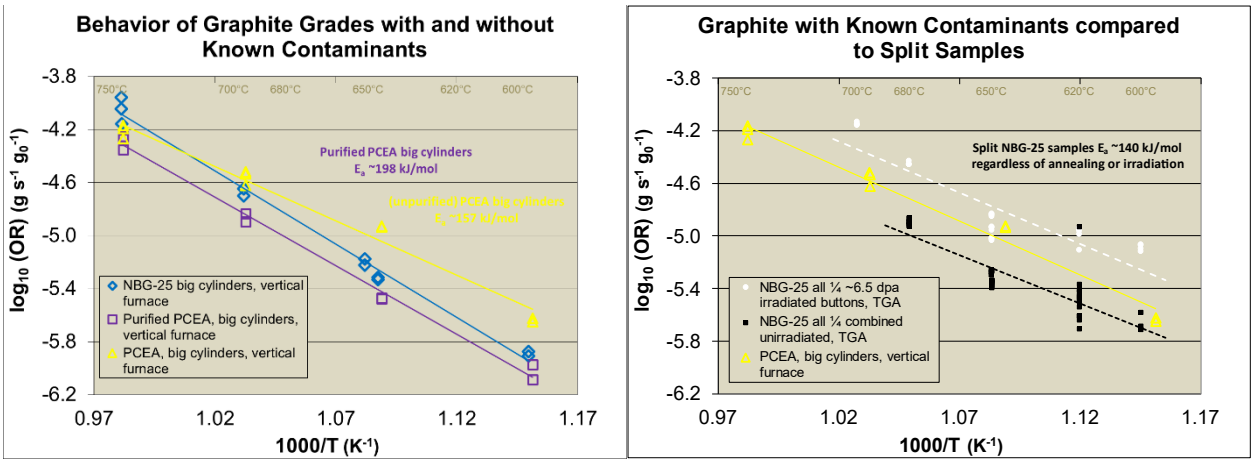

Figure 8. Comparison (at 5–10% mass loss, mass normalized) of PCEA graphite oxidized in the vertical furnace (with and without known impurities, left) to NBG-25 split sample performance in the TGA (with and without irradiation, right). Blue diamonds in both left and right graphs represent the same big cylinders oxidized in the vertical furnace.

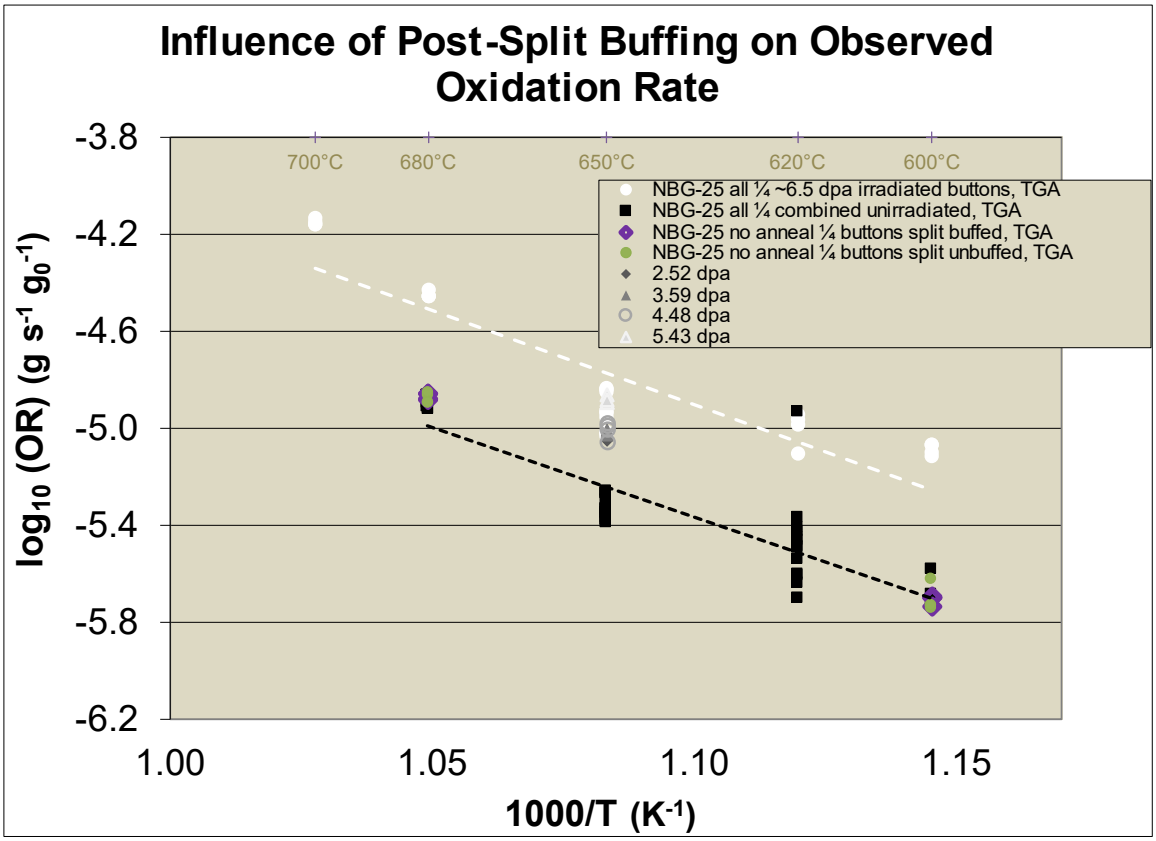

Figure 9. Oxidation data for buffed and unbuffed split samples of (unirradiated) NBG-25 superimposed on top of earlier (irradiated and unirradiated) split sample data.

Table 3. Comparison of Average Oxidation Behaviors at the Two Temperature Extremes.

Oxidation Temperature (°C)	Test Objective	Mass Normal Oxidation Rate over 5-10% mass loss ($g\ s^{-1}\ g_0^{-1}$)		
		By Test Run	Average	Standard Deviation
600	No Irradiation, No Anneal Split Sample Not Buffed	2.37232E-06	1.96E-06	2.7E-07
		1.79711E-06		
		1.8448E-06		
		1.84514E-06		
	No Irradiation, No Anneal Split Sample Buffed	1.99401E-06	1.97E-06	8.3E-08
		2.02332E-06		
		2.00911E-06		
		1.84405E-06		
	Companion (AGC-3), not irradiated, with and without anneal	*	2.21E-06	3.6E-07
		2.61675E-06		
		1.95407E-06		
		2.05852E-06		
	AGC-1, 6.78 dpa at 678.5°C, with and without anneal	7.99568E-06	8.18E-06	4.5E-07
		8.53836E-06		
		8.55614E-06		
		7.64061E-06		
680	No Irradiation, No Anneal Split Sample Not Buffed	1.35745E-05	1.32E-05	6.1E-07
		1.27572E-05		
		1.39324E-05		
		1.27014E-05		
	No Irradiation, No Anneal Split Sample Buffed	1.3813E-05	1.35E-05	3.7E-07
		1.31166E-05		
		1.38021E-05		
		1.32092E-05		
	Companion (AGC-1), not irradiated, with and without anneal	1.35838E-05	1.27E-05	6.7E-07
		1.37071E-05		
		1.27029E-05		
		1.22559E-05		
		1.28469E-05		
		1.27761E-05		
		1.18922E-05		
		1.20014E-05		
	AGC-1, 6.36 dpa at 658°C, with and without anneal	3.72105E-05	3.56E-05	1.1E-06
		3.50107E-05		
		3.50628E-05		
		3.50614E-05		

* One split was inadvertently oxidized at the wrong temperature setting and therefore was not included here.

4.2 Oxidation Rate Calculation Methodology

The method for calculation of the oxidation rate based on measured mass loss was adopted directly from the *Standard Test Method for Air Oxidation of Carbon and Graphite in the Kinetic Regime* (ASTM D7542). The practices described favor normalization by surface area to discriminate subtle performance variations among specimens of the same nominal size and shape but allow for mass or volume normalization to suit the user's application. While the Arrhenius relationship holds for any consistent mass loss range, 5–10% is specified for robust reproducibility among variations in equipment and users. And the percent mass loss is to be based upon the mass measured in flowing gas at temperature to account for the effects of buoyancy and drag on the suspended sample.

This methodology was developed for larger samples tested in a vertical furnace system, and primarily for comparison of oxidation performance among disparate graphite sources. For split samples (or even whole button samples) in a TGA, no standard yet exists. So, the application of each practice needs to be reviewed in this context.

4.2.1 Choice of Normalization

The initial choice for normalization of split sample oxidation rate data was obviated by the awkward shape of the sample. Absent reliable measurements for surface area and volume dimensions of the individual split pieces, all data were mass normalized. Previous efforts with whole button and big cylinder samples seemed to support this strategy (Smith 2019).

As a secondary option, surface area and volume estimates have been made based on some simplifying assumptions. The volume of each split was estimated on the assumption that it had the same initial density as the parent button for which the necessary mass and dimensional data (height, external diameter, and internal diameter) were available. Calculating split sample surface area requires a uniform density assumption, and more.

Estimating the initial surface area of a split sample assumes that the surfaces of the split sample are approximated as the cylindrical sector with exterior diameter of the parent button less the cylindrical sector of the axial hole in the parent button and arc lengths that give a solid volume with the same density as the parent button. Parent button and split are assumed to have the same height. Then it follows that the ratios of split arclength to parent circumference (for both the outer and inner sector of the split sample) are the same as the ratio of split sample mass to parent button mass. While these assumptions are not optimal, they do provide a framework for reassessing the Arrhenius plots for comparison of the split samples to larger samples.

4.2.2 Choice of Mass Loss Range

At the incrementally small range of initial onset, given equivalent environmental conditions, one would expect the graphite oxidation rate (of the same grade of material) to be proportional to the exposed surface area of the graphite article regardless of size or aspect ratio. However, the TGA and vertical furnace systems cannot accurately establish the rate of oxidation precisely at initial onset: the gas transition (from nitrogen to air) takes time and mass loss must progress far enough to be reliably detected. This initial change in mass must also be distinguished from buoyancy and drag effects: the measured weight of a sample at temperature in flowing gas varies slightly from the weight measured in still air under ambient conditions. Furthermore, if the mass loss range is not wide enough or too wide, reproducibility may suffer—small variations can have an outsized effect on the calculated rate if the selected range is too wide or too small. Similarly, the sampling rate (for data collection) may also constrain accurate and reproducible determination of oxidation rate due to the transient nature of onset. As the extent of reaction progresses, a density gradient evolves, depending on the local conditions within

the microstructure. The density gradient expresses the nonuniform influences of both surface area and volume.

Given the practical test considerations and the sigmoidal shape of mass loss plotted over time as the graphite is oxidized from onset to ash, the 5–10% range is a reasonable compromise for a 25-mm-diameter test sample. This range is far enough beyond the initial onset to approach quasi-steady state. The nearly constant reaction rate within (and just outside) this range means small variations in the calculation or limited sampling for data collection change the calculated oxidation rate relatively little.

The mass loss curves for the split samples, while often limited to 10% total mass loss, did not exhibit much deviation in quasi-steady state linearity over the 5–10% mass loss range originally assessed. Although oxidation progressed much more rapidly as a fraction of the initial mass, no discontinuities or aberrations in curve shape were observed for split samples by comparison to the same grade of big cylinders. In the interest of understanding and enabling a more meaningful comparison between these two disparate geometries, Arrhenius plots for the unirradiated split samples and the big cylinders were screened using each normalization variant and across the following mass loss ranges: 0–0.05%, 0.05–0.1%, 0–0.5%, 0.1–0.5%, 0.5–1%, 0.1–3%, 0.5–3%, 1–3%, 3–5%, and 5–10%, Figure 10. Note that, to reduce the scope of data processing required to complete this set of calculations, the separately sourced split sample data have been omitted from Figure 10.

This exercise suggests that the alteration to the effective activation energy may be an artifact of the rate calculation methodology rather than the presence of catalytic contaminants. Also, while surface area normalized rate data for non-irradiated samples largely converge for the smallest interval near initial onset regardless of geometry, irradiated (~6.5 dpa) split samples show consistently lower oxidation rates than their non-irradiated companions until ~0.5% mass loss. (Companion samples achieved 0.5% mass loss after 0.61 hour at 650°C on average while those irradiated samples with ~6.5 dpa exposure required 0.99 hour to reach 0.5% mass loss under the same conditions). Observe that for the limited 0.1–0.5% mass loss range, the oxidation rate shows no meaningful difference between the oxidation rates of irradiated and unirradiated splits, regardless of choice of normalization. Beyond 0.5% mass loss, up to the 10% mass loss for which data are available, irradiated splits show progressively faster oxidation relative to the companion splits.

The reduction in oxidation rate for irradiated split samples relative to their non-irradiated companions near initial onset suggests that the reduced porosity associated with radiation-induced dimensional changes dominates the irradiation effect on rate near onset. However, irradiation-induced defects seem to have increased the initial (pre-oxidation) concentration of active sites, a factor magnified by the progression of the oxidation reaction, as the cascade of the reaction further increases the availability of active sites until quasi steady state. Consequently, initial onset is slower, but the approach to quasi steady state that follows is faster and both factors depend on dose, exhibiting the nominal 10% increase in rate for each 1 dpa for the NBG-25 material over the first 10% of mass loss.

The surface area normalized temperature dependence of the oxidation rate for split samples over the 5–10% range of mass loss was observed to be nearly identical to the big cylinders over the 0.1–0.5% mass loss range. While this was initially thought to offer a potentially useful corollary for understanding and modeling oxidation rate behavior across differing geometries and flow conditions, it seems less helpful in the broader context of Figure 10. While only a single grade of graphite material is shown in Figure 10, surface-area-normalized graphite behaviors (excepting those with catalytic contaminants or irradiation histories) generally converge near onset (see Figure 11). However, the effect of duration (extent of reaction) and the effect of sample geometry both appear to be directly coupled to the surface-area-to-volume-ratio as long as adequate oxidant is provided and other parameters are maintained (meaning that, to a good approximation, kinetic regime behavior applies even for the different geometries and test systems used).

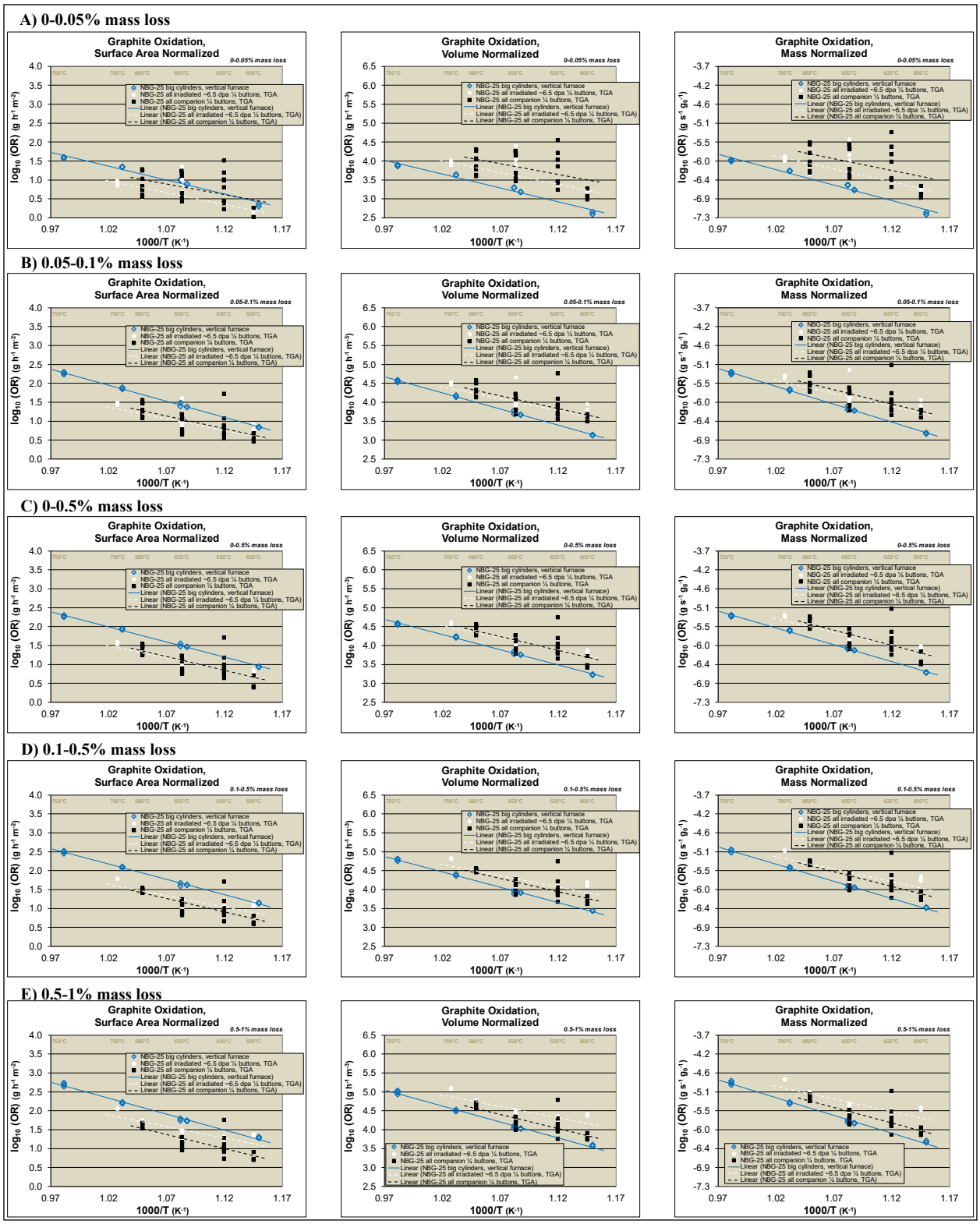

Figure 10. (A thru E). Calculation methodology adapted to compare NBG-25 split samples to NBG-25 big cylinders, A) over 0–0.05%, B) over 0.05–0.1%, C) over 0–0.5%, D) over 0.1–0.5%, and E) over 0.5–1% mass loss, surface area normalized (left), volume normalized (center), and mass normalized (right) (figure continues next page).

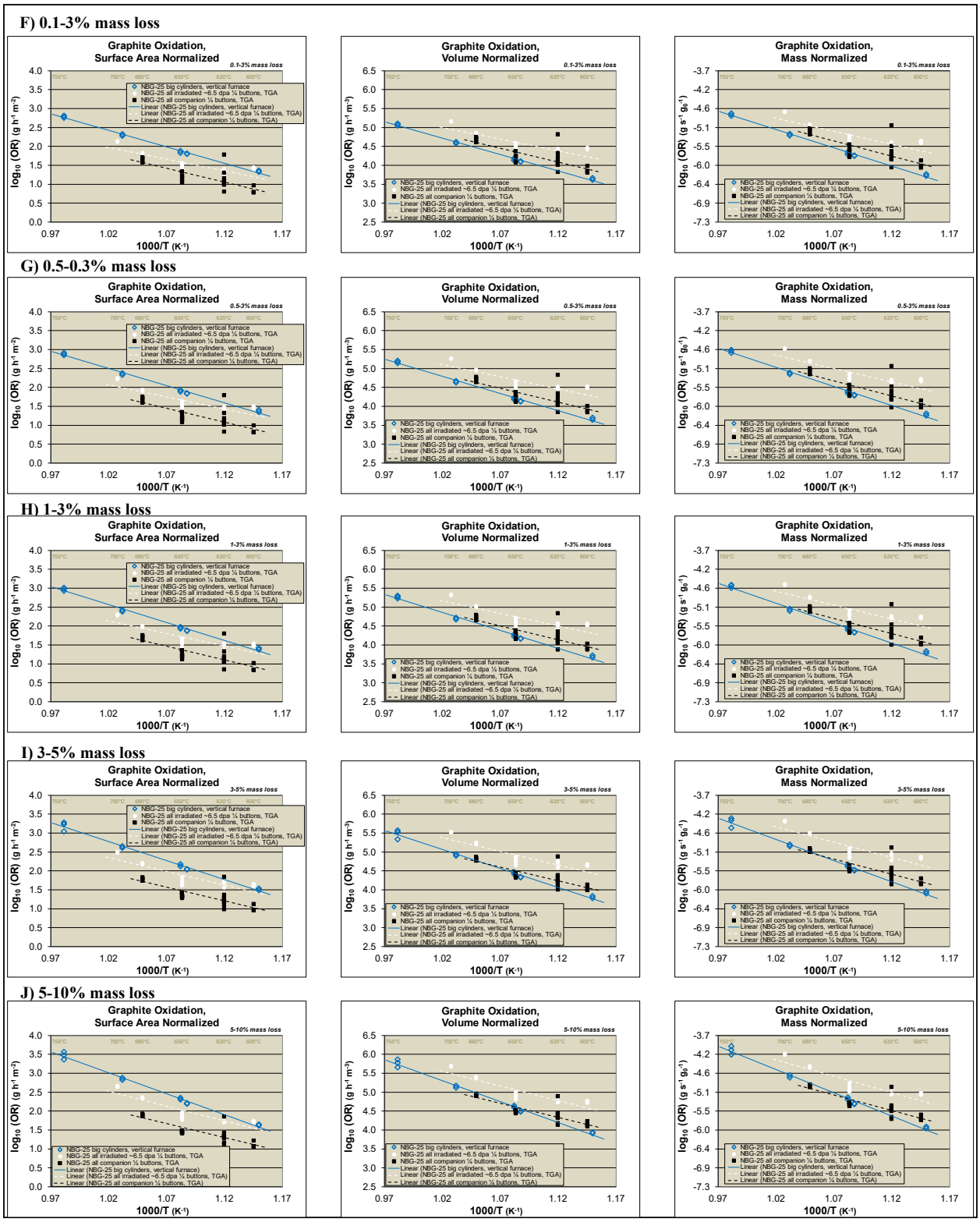

Figure 10 (F thru J). Calculation methodology adapted to compare NBG-25 split samples to NBG-25 big cylinders, F) over 0.1–3%, G) over 0.5–3%, H) over 1–3%, I) over 3–5%, and J) over 5–10% mass loss, surface area normalized (left), volume normalized (center), and mass normalized (right, continued from previous page.)

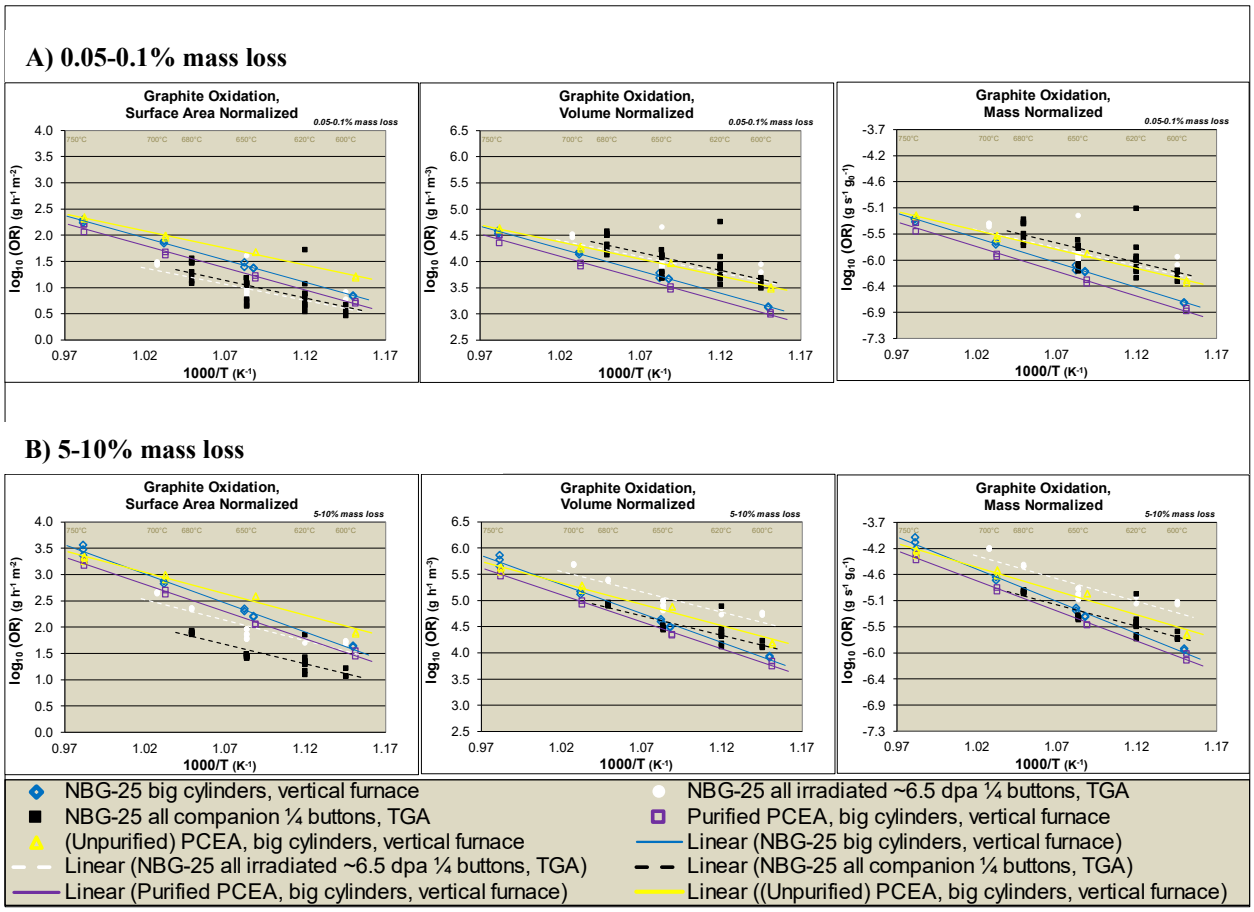

Figure 11. Calculation methodology adapted to compare NBG-25 split samples to NBG-25 big cylinders, including both (unpurified) PCEA and Purified PCEA, A) over 0.05–0.1% mass loss and B) over 5–10% mass loss, surface area normalized (left), volume normalized (center), and mass normalized (right).

4.2.3 Accounting for Buoyancy and Drag Effects

Revisiting the data for split sample test runs to screen the normalization and mass loss range variations also revealed an inconsistency in accounting for buoyancy and drag effects for some of the test runs. In every case the mass at start of oxidation was selected as an average weight measured at temperature (and gas flow), conditions immediately before the transition from nitrogen to air. However, in numerous cases the stabilization time at temperature before the gas transition was of inadequate duration, with the gas transition immediately followed the temperature ramp (to minimize the potential for unintentional annealing). This inconsistency in TGA operating protocol likely contributed to the observed scatter in the split sample data. The previously noted extreme outlier not only fit this pattern but also overshot the target oxidation temperature by nearly 8°C (after gas transition to air) and required slightly longer than other runs to settle back at the temperature setpoint.

4.3 TGA Operating Variables

In addition to the button splitting practices and the possibility of sample contamination, the operation of the TGA was performed by multiple staff members over the course of this work. While the intention was always to handle the test specimens in a consistent and well-documented manner, changes in personnel and requirements for conduct of research within a radiological control area challenged that objective. As there were some missteps in programming the TGA for adequate stabilization time at temperature before the introduction of air for some runs, there may also have been other discrepancies in

TGA operation that escaped documentation, or that otherwise went unnoticed. Consequently, the primary TGA operating parameters are outlined below.

The TGA output typically includes four columns of data: run time, thermocouple temperature output, sample mass, and a preliminary percent mass based on the first mass measurement made by the instrument. The preliminary percent mass functions as an operator aid for determination of whether or how soon the run can be completed with at least 10% mass loss.

There is high confidence that the TGA operated at 200 mL/minute environmental gas flow because this parameter was generally included in the TGA output filename, and participants were aware of other recent efforts to benchmark TGA oxidation against oxidation in the vertical furnace. Attention was on both maintaining suitable excess of oxidant and testing at sufficiently low temperatures that the oxidation behavior in the TGA would be controlled by reaction kinetics rather than unduly influenced by diffusion. The TGA also has a protective helium counterflow which deflects the chamber exit gas away from sensitive components of the instrument but should not affect the environment at the sample. For air oxidation testing, this counterflow has conventionally been set at 5 mL/minute.

Challenges associated with programming the TGA sampling rate are possible, and there can be difficulties both with sampling too frequently and too seldom. For example, some of the data files for low temperature tests of whole buttons in the TGA needed to be reduced by a factor of 10 or more to produce spreadsheet files of manageable size for analysis because sampling was too frequent. Minimal loss of resolution occurred because the change in mass was slow. The greater concern is sampling too seldom since rapid rate changes indicated by weight changes would not be captured. However, this did not appear to be a problem with the split samples. Split sample runs recorded data every 10 seconds regardless of other run parameters. The highest temperature split sample tests with the most rapid oxidation still required at least 1½ hours for 10% mass loss, and even the lowest temperature runs achieved 10% mass loss in less than 24 hours. At both extremes the graphs plotting mass loss against time showed smooth, continuous curves, so there is no indication that a higher or lower sampling rate was needed.

5. CONCLUSIONS

Regardless of the observed scatter, these data were carefully controlled, are self-consistent, and show a clear and significant increase in the rate of oxidation of NBG-25 with neutron dose. Dose dependency suggests a 10% increase in oxidation rate for each 1 dpa, with a dose of ~6.5 dpa doubling or tripling the rate of oxidation (depending on temperature) for unirradiated same-source material. However, even with accelerated oxidation at the highest temperatures and dose exposures tested, the oxidation reaction was not self-sustaining (no burning) (Windes 2014). The observed reduction in oxidation rate near onset and subsequent increase in rate with the approach to quasi steady state oxidation confirms that irradiation can both impede and accelerate oxidation by comparison to unirradiated same grade material. Furthermore, these results affirm the value of quartering button samples to maximize the oxidation test matrix, even without a quantitative method for scaling the observed behavior directly to larger articles of graphite.

6. REFERENCES

ASTM D7542, 2021, *Standard Test Method for Air Oxidation of Carbon and Graphite in the Kinetic Regime*. 2021. Accessed July 20, 2022. (West Conshohocken, PA: ASTM International, approved November 17, 2021) https://compass.astm.org/document/?contentcode=ASTM%7CD7542-21%7Cen-US.

Chi, S. -H., and G. C. Kim, 2021, "Effects of air flow rate on the oxidation of NBG-18 and NBG-25 nuclear graphite," *Journal of Nuclear Materials* 491, (August 2017): 37–42. https://doi.org/10.1016/j.jnucmat.2017.04.032.

Chinnathambi, K., J. J. Kane, D. P. Butt, W. E. Windes, and R. Ubic, 2015, Neutron irradiation induced microstructural changes in NBG-18 and IG-110 nuclear graphites, *Carbon* 86 (2015), pp. 124-131. http://dx.doi.org/10.1016/j.carbon.2015.01.036.

Contescu, C. I., S. Azad, D. Miller, M. J. Lance, F. S. Baker, and T. D. Burchell, 2008, "Practical aspects for characterizing air oxidation of graphite," *Journal of Nuclear Materials* 381, (October 2008): 15–24. https://doi.org/10.1016/j.jnucmat.2008.07.020.

Contescu, C. I., J. P. Strizak, T. R. Guldan, and T. D. Burchell, 2010, Effect of air oxidation on pore structure development and mechanical properties of nuclear graphite, ORNL/TM-2010/197, Oak Ridge National Laboratory, Oak Ridge, TN, 2010. https://doi.org/10.2172/1760103.

Contescu, C. I., 2011, Microstructure effect on air oxidation behavior of three nuclear grade graphite materials: NBG-18, PCEA, and IG-110, ORNL/TM-2011/324, Oak Ridge National Laboratory, Oak Ridge, TN (United States) 2011.

Dahl, R.E., 1961, "Oxidation of Graphite under High Temperature Reactor Conditions," Hanford Atomic Products Operation, UC-4, TIC-4500, HW-68493. https://doi.org/10.2172/4798328.

Kane, J. J., C. I. Contescu, R. E. Smith, G. Strydom, and W. E. Windes, 2017, "Understanding the reaction of nuclear graphite with molecular oxygen: Kinetics, transport, and structural evolution," *Journal of Nuclear Materials* 493, (September 2017): 343–367. https://doi.org/10.1016/j.jnucmat.2017.06.001.

Kelly, B. T., B. J. Marsden, K. Hall, D. G. Martin, A. Harper, and A. Blanchard, Irradiation damage in graphite due to fast neutrons in fission and fusion systems, IAEA-TECDOC-1154, International Atomic Energy Agency, Vienna, Austria, September 2000. https://www-pub.iaea.org/MTCD/Publications/PDF/te_1154_prn.pdf.

Kim, E. S., K. W. Lee, and H. C. No, 2006, "Analysis of geometrical effects on graphite oxidation through measurement of internal surface area," *Journal of Nuclear Materials* 348, (January 2006): 174–180. https://doi.org/10.1016/j.jnucmat.2005.09.018.

Kosiba, W. L., and G. J. Dienes, 1959, "The Effect of Radiation on the Rate of Oxidation of Graphite," US/UK Graphite Conference, St. Giles Court, London, December 16-18, 1957, pp. 121-132, Brookhaven National Laboratory, issued March 1959.

Kelly, B. T., B. J. Marsden, K. Hall, D. G. Martin, A. Harper, and A. Blanchard, 2000, Irradiation damage in graphite due to fast neutrons in fission and fusion systems, IAEA-TECDOC-1154, International Atomic Energy Agency, Vienna, Austria, September 2000. Accessed July 20, 2022. https://www-pub.iaea.org/MTCD/Publications/PDF/te_1154_prn.pdf.

Schweitzer, D. G., and E. M. Singer, 1965, Oxidation rates of alternately irradiated and annealed graphite, *Journal of Nuclear Materials* (1965): 220–226. https://doi.org/10.1016/0022-3115(65)90055-3.

Smith, R. E., 2019, "Comparison of Oxidation Performance of Graphite Samples in TGA versus Vertical Furnace," INL/EXT-19-54584, Idaho National Laboratory, Idaho Falls, ID, July 2019.

Smith, R. E., J. J. Kane, and W. E. Windes, 2020, "Determining the acute oxidation behavior of several nuclear graphite grades," *Journal of Nuclear Materials* 545, (March 2020): 152648. https://doi.org/10.1016/j.jnucmat.2020.152648.

Wichner, R. P., T. D. Burchell, and C. I. Contescu, "Penetration depth and transient oxidation of graphite by oxygen and water vapor," *Journal of Nuclear Materials* 393, (September 2009): 518–521. https://doi.org/10.1016/j.jnucmat.2009.06.032.

Windes, W., G. Strydom, R. Smith, and J. Kane, 2014, "Role of Nuclear Grade Graphite in Controlling Oxidation in Modular HTGRs," INL/EXT-14-31720, Idaho National Laboratory, 2014, https://doi.org/10.2172/1167529.

Zherdev F. F., I.E. Komissarov, B. A. Gurovich, and V. M. Markushev, 1992, "The effect of neutron irradiation on the reactor graphite corrosion kinetics." Journal of Nuclear Materials. 1992; 189(3):333–342. https://doi.org/10.1016/0022-3115(92)90386-Y.